Sulfonated microporous polymer membranes with fast and selective ion transport for electrochemical energy conversion and storage

RESEARCH ARTICLE

Sulfonated microporous polymer membranes with fast and selective ion transport for electrochemical energy conversion and storage

Peipei Zuo[a], Yuanyuan Li[a], Anqi Wang[b], Rui Tan[a], Yahua Liu[a], Xian Liang[a], Fangmeng Sheng[a], Gonggen Tang[a], Liang Ge[a], Liang Wu[a], Qilei Song*[b], Neil B. McKeown*[c], Zhengjin Yang*[a] and Tongwen Xu*[a]

[a] P.P. Zuo, Y.Y. Li, Y.H. Liu, X. Liang, F.M. Sheng, G.G. Tang, L. Ge, Prof. L. Wu, Prof. Z.J. Yang, Prof. T.W. Xu
CAS Key Laboratory of Soft Matter Chemistry, Collaborative Innovation Center of Chemistry for Energy Materials
School of Chemistry and Material Science, University of Science and Technology of China
Hefei 230026, P.R. China
E-mail: yangzj09@ustc.edu.cn, twxu@ustc.edu.cn

[b] A.Q. Wang, R. Tan, Dr. Q.Song
Barrer Centre, Department of Chemical Engineering
Imperial College London
London SW7 2AZ, U.K.
E-mail: q.song@imperial.ac.uk

[c] Prof. N.B. McKeown
EastCHEM School of Chemistry
University of Edinburgh
David Brewster Road, Edinburgh EH9 3FJ, U.K.
E-mail: neil.mckeown@ed.ac.uk

Supporting information for this article is given via a link at the end of the document.

Abstract: *Membranes with fast and selective transport of protons and cations are required for a wide range of electrochemical energy conversion and storage devices, such as proton-exchange membrane (PEM) fuel cells and redox flow batteries. Here we report a new approach to designing solution-processable ion-selective polymer membranes with both intrinsic microporosity and ion-conductive functionality. This was achieved by synthesizing polymers with rigid and contorted backbones, which incorporate hydrophobic fluorinated and hydrophilic sulfonic acid functional groups, to produce membranes with negatively-charged subnanometer-sized confined ionic channels. The facilitated transport of protons and cations through these membranes, as well as high selectivity towards nanometer-sized redox-active molecules, enable efficient and stable operation of an aqueous alkaline quinone redox flow battery and a hydrogen PEM fuel cell. This membrane design strategy paves the way for producing a new-generation of ion-exchange membranes for electrochemical energy conversion and storage applications.*

Introduction

With the fast development of renewable energy sources such as wind and solar power, there is a rapidly growing demand for electrochemical energy storage and conversion technologies to balance the intermittent energy supply and stabilize the power grid[1]. Several electrochemical processes hold great promise for large scale renewable energy conversion and storage, such as redox flow batteries (RFB),[2] electrolyser to produce H_2 fuel,[3] and fuel cells to convert the renewable H_2 back to electricity.[4] In these electrochemical devices, ion-conductive membranes are crucial components that enable fast transport of charge-carrying ions and isolate the chemical reactions in separate electrodes, which determine the system performance in terms of efficiency and stability. Low-cost and high-performing membranes with high ion conductivity and high selectivity are highly desirable for the large-scale applications of these electrochemical systems.[5]

Currently, commercial perfluorosulfonic acid membranes such as Nafion are the benchmark membranes used in PEM fuel cells and redox flow batteries owing to their high ionic conductivity, high chemical stability, mechanical strength, and desirable chemical and physical properties for electrochemical devices.[6] However, Nafion membranes are very expensive, the high cost of up to \$500/m^2 is limiting the large-scale development of a wide range of electrochemical processes. Over the past 30 years, the membrane community has devoted intensive efforts to developing low-cost hydrocarbon-based polymer membranes.[7] A variety of sulfonated polymers have been developed as cation exchange membranes using principles similar to those of Nafion membranes in that phase separation of hydrophobic backbone and hydrophilic side-chains form hydrophilic domains.[7] The architecture of these hydrophilic domains is very challenging to control so that the size of hydrophilic domains is too large to ensure sufficient selectivity towards redox actives species in electrolytes, which leads to battery decay and poor cycling stability.

Recent development of microporous polymers such as Polymers of Intrinsic Microporosity (PIMs) provides a new platform for designing ion-exchange membranes with molecularly-defined pore structures and size-exclusion function that enable fast and selective ion transport.[8] Previous work on ion transport PIMs has been focused on PIM-1 and application in organic solvent electrolytes.[9] In addition, we reported a new generation of anion-exchange membranes derived from Tröger base-containing PIMs,[10] and demonstrated the fast transport of hydroxide and chloride anions through the subnanometer cavities

within the positively charged polymer membranes. Recent work also demonstrated that hydroxide exchange membranes and ionomers prepared from rigid backbones present improved ionic conductivity as well as high stability.[11] It is highly desirable to manufacture cation-exchange PIM membranes for PEMFC and RFB applications. However, it remains challenging to prepare sulfonated PIM polymers due to difficulties such as material degradation or the formation of insoluble gels, encountered during synthesis.[12]

Here, we report the preparation of a new generation of sulfonated microporous polymer membranes with rapid and selective transport of protons and cations in redox flow batteries and fuel cells. As schematically shown in Figure 1a, the sulfonated polymers with rigid and contorted backbones prohibit conformation change and disrupt efficient packing of polymer chains, creating subnanometer cavities and confined channels that enable fast transport of protons and cations. Owing to the rigidity of the polymer chains incorporated with hydrophobic fluorinated functional groups, the resulting membranes show a limited degree of phase separation and swelling. The sulfonated microporous polymer membranes enable fast transport of protons and potassium ions and high selectivity towards nanometer-sized redox-active organic molecules and ferrocyanide ions due to a combination of size exclusion, electrostatic interaction and repulsion. We further demonstrate that these highly conductive membranes enable high performance of electrochemical devices, including an organic redox flow battery using 2,6-dihydroxyl anthraquinone (DHAQ) and $K_4[Fe(CN)_6]$ as redox couple, and a PEM fuel cell using H_2 fuel. We expect that our membrane design concept will inspire the rational design of a new generation of cation exchange membranes that will support the large-scale adoption of electrochemical energy conversion and storage devices.

Our design strategy of using rigid partially fluorinated backbone limits the conformational freedom of polymer chains, prevents the polymer chains from packing tightly and frustrates the aggregation of sulfonic acid groups, creating confined ionic channels in a solution-processable membrane (Figure 1b and 1c). To achieve this design strategy, we use recently reported PIMs based on polyxanthene chemistry for the synthesis of precursor microporous polymers.[13] The sulfonated polymer membranes are prepared by (1) synthesis of precursor polyxanthene-based polymers with rigid and contorted backbone, (2) incorporation of fluorinated groups to improve the hydrophobicity of backbone, and (3) controlled sulfonation. Two polyxanthene-based PIM polymers, termed as PX-BP and PX-HFP, were synthesized through superacid catalyzed polymerizations using commercially available monomers α,α,α-trifluoroacetophenone and 4,4′-(hexafluoroisopropylidene) diphenol (forming PX-HFP, Figure 1d and 1e), or 4,4'-dihydroxybiphenyl (forming PX-BP, Figure 1f and 1g), respectively (Figure S1). The efficient polymerization reaction yields polymers with high molecular weight suitable for casting mechanically robust membranes (Figure S2). The resulting polymers were then sulfonated with chlorosulfonic acid, forming polymers termed as SPX-BP and SPX-HFP (Figure 1d and 1f, Figure S3 and S4), after which the polymers are readily soluble in polar organic solvents, e.g. dimethylformamide, *N*-methyl-2-pyrrolidone and dimethyl sulfoxide (Figure S5). The degree of sulfonation or the sulfonic moiety content, i.e. ion exchange capacity (IEC, mmol g^{-1}), as determined by titration, can be tuned by controlling the reaction time and the amount of chlorosulfonic acid used. The rigid backbone and partially fluorinated polymer structure enable the polymer to be chemically stable and soluble in common organic solvents both before and after sulfonation, which is a significant achievement for making ion selective PIM membranes.

To understand the pore structures of the pristine polymers and those of the sulfonated polymers, we performed gas adsorptions and molecular simulations. Molecular modelling predicted that the as-synthesized polymers and sulfonated polymers present subnanometer-sized cavities (Figure 1b, Figure S6). Nitrogen (N_2) adsorption-desorption measurements of unmodified polymer samples at 77 K confirm that PX-HFP has an apparent BET surface area of 146 $m^2 g^{-1}$, while PX-BP has a higher value of 389 $m^2 g^{-1}$ (Figure 1h, Figure S7), which corresponds to its more rigid structure (Figure 1e and 1g, Figure S6). The obvious hysteresis between adsorption and desorption isotherms of PX-HFP indicates a kinetic barrier to adsorption suggesting that pores are poorly-connected. In contrast, PX-BP shows much higher adsorption of N_2 and less obvious hysteresis (Figure 1h). Adsorption measurements at 273 K using probe molecule of smaller kinetic diameter, CO_2, also showed that PX-BP exhibits a much higher adsorption capacity than PX-HFP (Figure 1i). We also measured gas sorption isotherms of two sulfonated polymers with low degree of sulfonation, SPX-HFP or SPX-BP. Both sulfonated polymers show negligible adsorption of N_2 at 77K, indicating an increase in inter-chain polymer cohesion owing to strong hydrogen-bonded interchain interactions as reported in other PIM polymers.[14] The amount of CO_2 adsorption at 273 K in sulfonated polymers is slightly increased over that in pristine polymers, presumably because of the polar interaction between sulfonic moieties and CO_2 molecules (Figure 1i) and the presence of smaller micropores. The pore size distribution profiles derived from CO_2 adsorption isotherms confirm that subnanometer-sized pores are still present in sulfonated polymers (Figure 1j).

The sulfonated polymer membranes were characterised range of techniques un order to understand their structure and properties. Thermal Gravimetric Analysis (TGA) showed that the polymers are thermally stable with decomposition temperature up to 300 °C (Figure S8). Stress-strain curves measured by dynamic mechanical analysis confirm that films of the polymers possess high mechanical strength with Young's modulus as high as 19.5 MPa (Figure S9). Fenton's test reveals that the sulfonated polymer membranes are chemically stable, retaining 98.5% of the original weight after immersion for 2 h at 80°C (Table S1), which is a challenging environment for most sulfonated aromatic polymers.[15] Wide-angle X-ray scattering (WAXS) of pristine polymer membranes present broad peaks corresponding to *d*-spacings in the range of 4-9 Å. After sulfonation, the broad peaks become weak suggesting that the polymer chain packing becomes denser owing to hydrogen-bonding (Figure S10). However, the average *d*-spacing of the relatively porous polymers SPX-BP, which is likely tob e more strongly hydrogen-bonded, is larger than that of dense nonporous polymers,[16] owing to the rigid and contorted polymer backbone structure.

The polymer membranes show increasing water uptake with a higher degree of sulfonation by dynamic vapor sorption (DVS) (Figure 2a). We further measured the bulk water uptake in these sulfonated polymer membranes by mass changes in dry and wet conditions (Figure 2b, Figure S11). The membranes derived from SPX-BP-0.95 demonstrates a bulk water uptake of around

30 wt% at all operating temperatures (Figure 2b). We hypothesize that the hydration of the membranes forms interconnected water channels suitable for ion transport.[17] Figure 2d shows the membranes in dry and wet conditions, with a low swelling ratio below 10% at temperature up to 80 °C as quantified by measuring their size change. In contrast, the benchmark Nafion 117 membrane exhibits much more obvious size change and higher water swelling (Figure 2c and 2d). Atomic force microscopy (AFM) under atmospheric conditions and humidity of about 45% show no distinct phase separation morphology of the sulfonated membranes, as opposed to that of Nafion 117 (Figure 2e, 2f and 2g). Combining the results obtained from gas adsorption experiments, WAXS, water uptake measurements, and AFM imaging, it appears that our newly-developed sulfonated polymer membranes possess narrow subnanometer pores in both dry and wet states, which are expected to facilitate the ion transport.

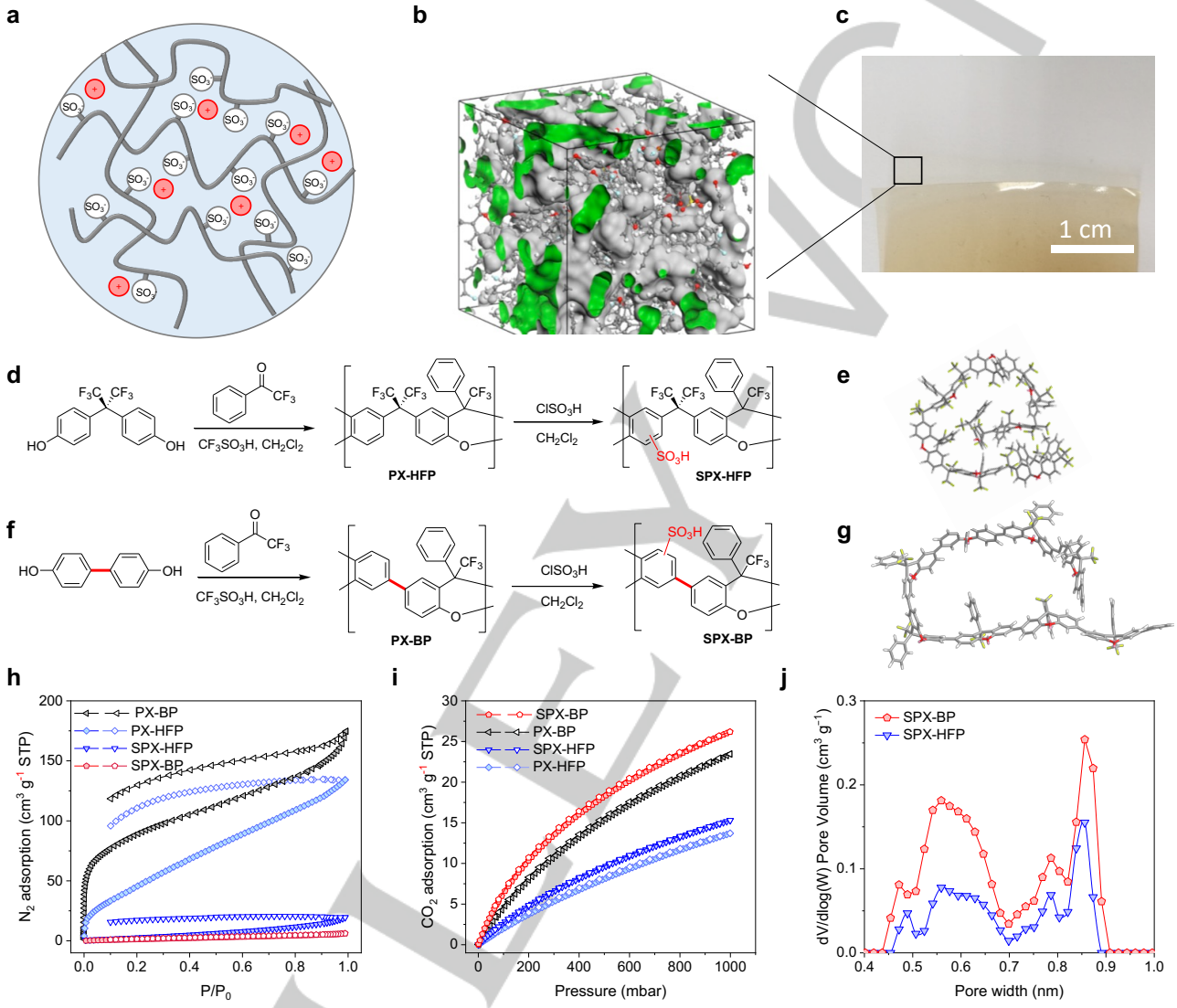

Figure 1. Cation exchange membranes from intrinsically microporous polymers. (a) Schematic illustration of a sulfonated polymer membrane from intrinsically microporous polymers used as cation conducting membrane. (b) The simulated amorphous cell of SPX-BP. Cell size: 25.73 Å × 25.73 Å × 25.73 Å. Green colour: accessible surface. (c) A photograph of SPX-BP membrane (size: 3.0 cm × 4.0 cm). The syntheses of PX-HFP (d) and PX-BP (f), which were then sulfonated by chlorosulfonic acid. A molecular model of PX-HFP (e) and PX-BP (g), showing the more rigid structure of PX-BP which generates intrinsic microporosity due to the inefficient chain packing in the solid state. (h) N_2 sorption isotherms of PX-HFP, SPX-HFP, PX-BP and SPX-BP (77.3 K). (i) CO_2 sorption isotherms of PX-HFP, SPX-HFP, PX-BP and SPX-BP (273 K). (j) Pore size distributions of SPX-HFP and SPX-BP from CO_2 sorption isotherms based on density functional theory (DFT) calculations assuming slit pore geometry.

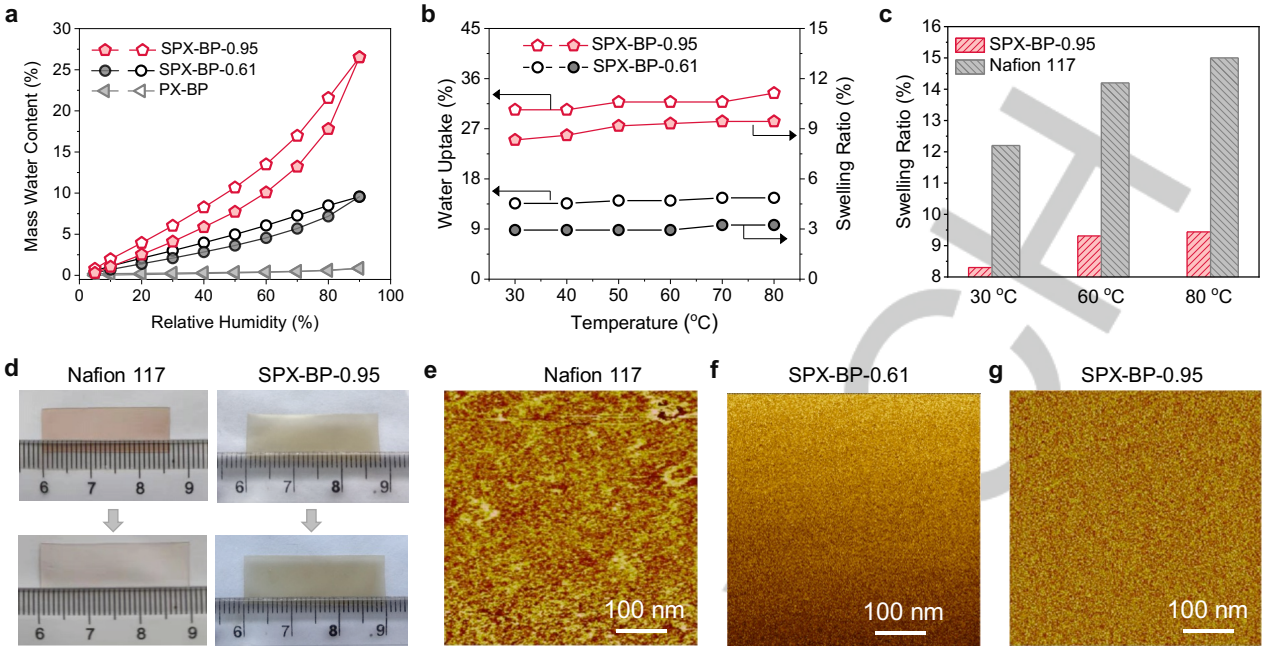

Figure 2. Characterizations of membranes. (a) Dynamic water vapor sorption isotherms of PX-BP, SPX-BP-0.61 and SPX-BP-0.95, measured at 25 °C. Water uptake and membrane swelling ratio of SPX-BP-0.61 and SPX-BP-0.95 (b) as functions of operating temperature. (c) Swelling ratio of SPX-BP-0.95 and Nafion 117 at varied operating temperature. (d) Photos showing the water swelling of Nafion 117 and SPX-BP-0.95 before and after immersion in water for 12 h at 25 °C. AFM phase images of Nafion 117 (e), SPX-BP-0.61 (f) and SPX-BP-0.95 (g), recorded under ambient conditions. The dark areas show the hydrophilic (ionic) domains, and the bright areas show hydrophobic domains. As in SPX-BP-0.61, 0.61 indicates the sulfonic moiety content (i.e. ion exchange capacity, IEC), in mmol g^{-1}.

Owing to the formation of narrowly distributed subnanometer channels and incorporation of sulfonic acid groups, the PIM membranes exhibited remarkable ionic conductivity. The proton conductivity of SPX-HFP-0.63 membrane at 30 °C is 7.6 mS cm^{-1}, which increases steadily to 18.8 mS cm^{-1} at 80°C. In contrast, for the relatively more porous SPX-BP-0.61 membrane, the proton conductivity is 26.9 mS cm^{-1} at 30 °C, and increases to 83.6 mS cm^{-1} at 80 °C, which is more than four times higher than that of SPX-HFP-0.63 at 80°C (Figure 3a), indicating that porosity plays a crucial role in enhancing the ionic conductivity.

To confirm the effect of porosity on ionic conductivity, we blended membranes consisting of different weight ratios of SPX-BP-0.61 and SPX-HFP-0.63. As the fraction of the microporous SPX-BP-0.61 increases, the resulting membranes exhibit higher proton conductivity (Figure 3a). Similar enhancement of potassium ion conductivity was observed in membranes with enhanced microporosity (Figure 3b). Conventional sulfonated polymer membranes usually display a linear relationship between the ionic conductivity and water uptake because the ion transport depends on the formation of water channels via phase separation.[18] In contrast, both SPX-BP-0.61 to SPX-HFP-0.63 have low ion exchange capacity (0.6 mmol g^{-1}) and similar water uptakes of ~14 wt% at 30 °C that changes only slightly at elevated temperatures (Figure 2b, Figure S11). Therefore, we attribute the enhanced transport of proton and potassium ions to the microporosity within SPX-BP-0.61.

To investigate the effect of sulfonation on ionic conductivity, we further tailored the degree of sulfonation of microporous polymer membranes. As the content of sulfonic moieties increases from 0.61 mmol g^{-1} to 0.95 mmol g^{-1}, the proton conductivity of SPX-BP membranes increases. For example, SPX-BP-0.95 with a relatively higher IEC of 0.95 mmol g^{-1} show significantly improved proton conductivity of up to 180 mS cm^{-1} at 80 °C (Figure 3c), which is comparable to that of membranes of the benchmark Nafion 117. The activation energy for proton transport decreases from 17.15 kJ mol^{-1} to 10.39 kJ mol^{-1} as the content of sulfonic acid groups increases (Figure S12), implying the formation of a more efficient proton transport network. The sulfonated microporous polymer membranes also exhibit high ion conductivity for small salt ions such as potassium (Figure 3d). For SPX-BP-0.95, nearly identical potassium ion conductivity, as determined in practical coin cells, is obtained as that of benchmark Nafion 117 in the temperature range of 30-80°C (Figure 3e). To compare our membranes with previously reported proton exchange membranes, we plot the proton conductivities versus IEC (Figure 3f). The SPX-BP membrane with a moderate amount of sulfonation, SPX-BP-0.95, shows comparable proton conductivity to that of benchmark Nafion 117 and outperforms a wide range of hydrocarbon proton exchange membranes with a high degree of sulfonation and high IEC (detailed conductivity values can be found in Table S2). Data for the SPX-BP membranes, along with that of Nafion117, are located in the region where high proton conductivity is obtained at very low IEC. Transport of protons and small alkali ions (such as potassium) through cation-exchange membranes is governed by structural diffusion or vehicular transport mechanism,[19] which is determined largely by the interconnectivity of the hydrated domains of the sulfonic moieties. Owing to their rigid, contorted and partially fluorinated backbone, our sulfonated microporous membranes possess a limited degree of conformational freedom and form nanoconfined inter-connected ionic channels that facilitate ion transport.

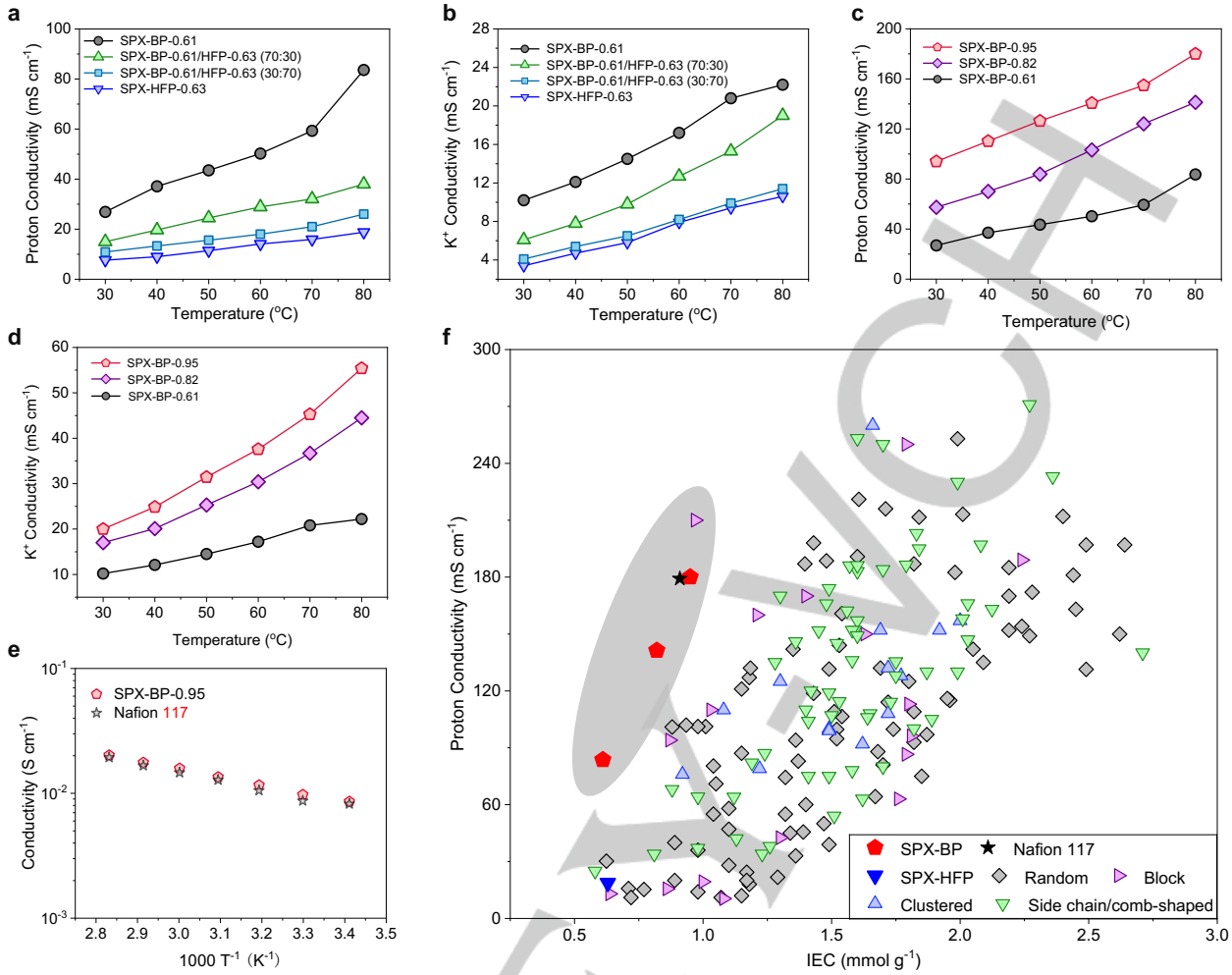

Figure 3. Ionic conductivity of sulfonated polymer membranes. (a) H^+ conductivity and (b) K^+ conductivity of solution cast standing-alone membranes from SPX-HFP-0.63, SPX-BP-0.61, and their blends as functions of operating temperature. (c) H^+ conductivity and (d) K^+ conductivity of solution cast standing-alone membranes from SPX-BP with varied sulfonic moiety content as functions of operating temperature. Conductivity was measured with a standard four-electrode electrochemical impedance spectroscopy (EIS) under fully humidified conditions. (e) Conductivity of SPX-BP-0.95 and Nafion 117 measured in a practical coin cell (Type 2032) via EIS. (f) A plot of H^+ conductivity versus IEC for representative proton exchange membranes, Nafion 117, SPX-HFP, and SPX-BP. SPX-BP membrane, along with the commercial benchmark Nafion 117 membrane, outperforms most of the previously reported membranes, delivering very high proton conductivity at low IEC. The proton conductivity values were reported or measured for fully hydrated membrane samples at 80 °C. Detailed conductivity values can be found in Table S2.

To investigate the ion diffusion through these ion-conductive membranes in aqueous electrolytes and flow batteries, we measured the permeability of ions and redox active molecules in a two-compartment diffusion cell. SPX-BP-0.95 with a thickness of 145 μm can rapidly and selectively transport potassium ions. The permeability of KOH through SPX-BP-0.95 is as high as 2.42×10^{-6} cm s^{-1} and 2.03×10^{-6} cm s^{-1} for KCl, which are about 7 and 4 times higher than those measured for a Nafion 117 membrane with a similar thickness of 178 μm, respectively (Figure 4a). The permeation rates of LiCl, NaCl and KCl across SPX-BP-0.95 follow the sequence LiCl<NaCl<KCl (Figure 4b and 4c), which are inversely related to the hydrated radius of the cations (Li^+ = 0.382 nm > Na^+ = 0.358 nm > K^+= 0.331 nm).[20] In contrast, the phenomenon of size sieving of monovalent cations is not observed in Nafion 117 membrane (Figure 4c, Figure S13 and Table S3). Sulfonated SPX-BP-0.61 membrane (IEC=0.61 mmol g^{-1}) shows slow permeation of potassium ion through the membrane over 6 h, whereas the K^+ permeability was increased sharply to 7.30×10^{-7} cm s^{-1} for SPX-BP-0.82 (IEC=0.82 mmol g^{-1}) and 2.03×10^{-6} cm $s^{-1}$for SPX-BP-0.95 (Figure S13). As the channel size approaches the radii of hydrated ions and the Debye length of aqueous salt solutions, the transport of ions is governed by both size-sieving and electrostatic charge interaction. We propose that K^+ transport is enhanced by the closer electrostatic interaction of K^+ with the negatively charged sulfonic moieties ($-SO_3^-$) within subnanometer channels as compared to that in Nafion 117, while the monovalent cation selectivity is due to size-sieving effect originated from the shape-persistent and defined subnanometer sized micropores.

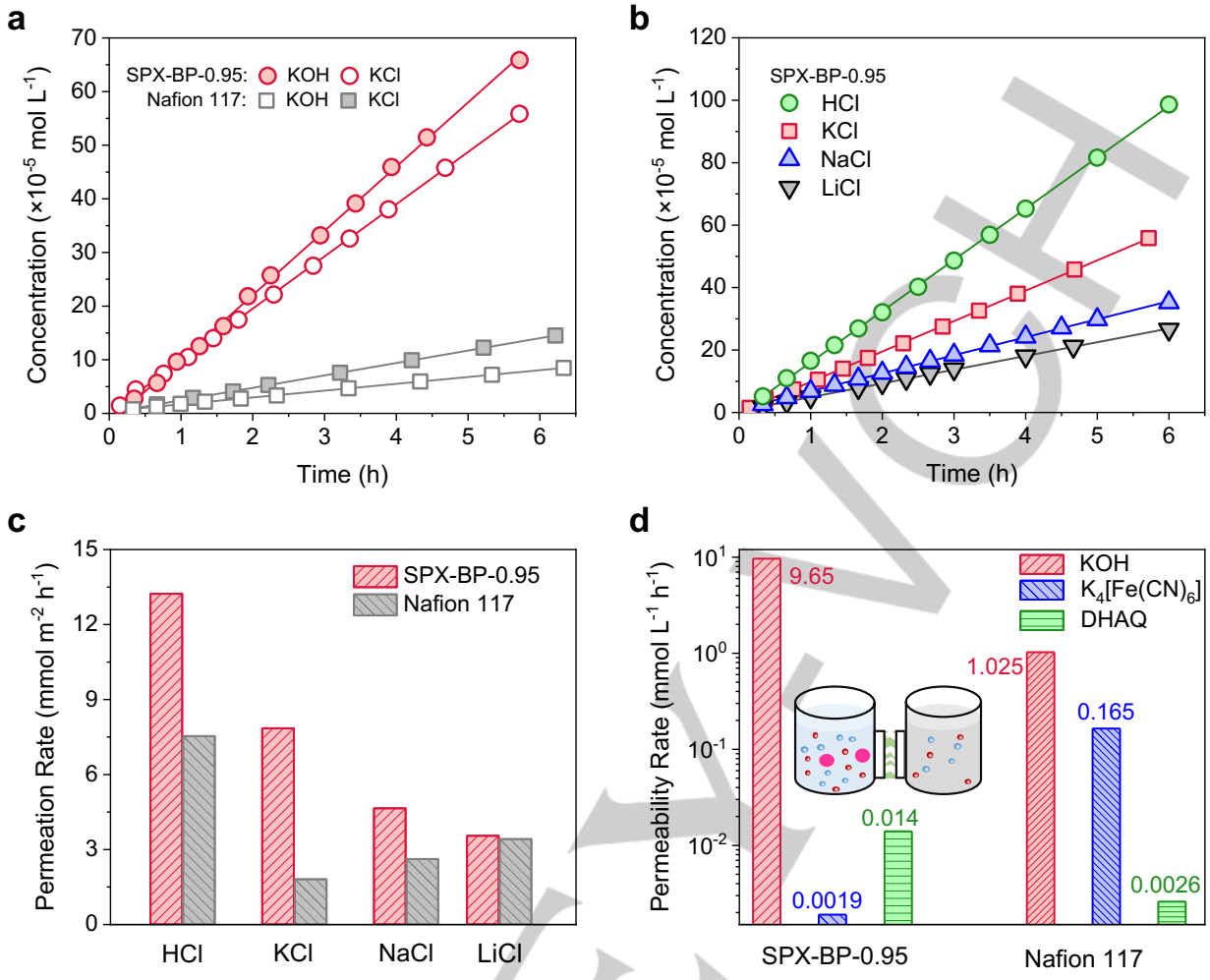

Figure 4. Ion diffusion and selectivity towards redox active molecules. (a) Diffusion of KOH and KCl through SPX-BP-0.95 and Nafi-on 117 measured in a two-compartment diffusion cell, where the donating side filled with 15 mL of 0.1 M KOH or KCl was separated from the receiving side (filled with 15 mL of deionized water) by either SPX-BP-0.95 or Nafion 117. (b) Diffusion of HCl, LiCl, NaCl or KCl through SPX-BP-0.95 measured in the two-compartment diffusion cells. Conductivity of the receiving side was monitored and calibrated. Deionized water in the lab has a conductivity of less than 2 μS cm^{-1}. (c) Permeation rates of HCl, LiCl, NaCl and KCl across SPX-BP-0.95 and Nafion 117. (d) Permeation rates of KOH, $K_4[Fe(CN)_6]$, and DHAQ across SPX-BP-0.95 and Nafion 117. Concentrations of the receiving side were determined by monitoring the conductivity, UV-vis adsorption or via inductively coupled plasma (ICP) and calibrated. Permeation rate or permeability was calculated by fitting the data to Fick's first law.

SPX-BP-0.95 selectively transports cations, while rejecting anions, for instance, OH^-, Cl^-, $[Fe(CN)_6]^{4-}$ and the dianion of 2,6-dihydroxyl anthraquinone ($DHAQ^{2-}$), which are all of relevance to applications in aqueous RFB. The calculated diffusion of K^+ and OH^- through the matrix of SPX-BP-0.95 was estimated by MD simulations. Mean square displacements of K^+ and OH^- reflect that K^+ can diffuse freely over time through the subnanometer cavities, while OH^- movement was restricted (Figure S14). The transference number (t_+), defined as the ratio of the electric current derived from cations to the total electric current,[21] was measured in a two-compartment diffusion cell, compartments of which were separated by SPX-BP-0.95 and filled with 0.1M/0.05M KCl solution. SPX-BP-0.95 membrane presents a high transference number of 0.997 (close to unity for an ideal cation selective membrane), implying the predominant contribution of K^+ over Cl^- on the total electric current, while similar measurement on benchmark Nafion 117 membrane yields a transference number of 0.982 (Table S4). As mentioned above, the permeation of KOH and KCl across SPX-BP-0.95 is likely to be affected by the rejection of anions by SPX-BP-0.95 membrane, due to the electrostatic repulsion of anions by the negatively charged sulfonic moieties and the small subnanometre pore size similar to the the Debye length of 0.1 M KCl solution.[22] The diffusion of larger anions, $[Fe(CN)_6]^{4-}$ and $DHAQ^{2-}$, was greatly impeded, with permeation rates of 1.90×10^{-3} mmol m^{-2} h^{-1} and 1.40×10^{-2} mmol m^{-2} h^{-1}, respectively (Figure 4d, Figure S15 and Table S3). This results very high selectivity of K^+ over $[Fe(CN)_6]^{4-}$ of up to 5079 and remarkably high selectivity of 690 for K^+ over $DHAQ^{2-}$ anions, with both values higher than those for Nafion 117 membranes (6.4 and 392, respectively).

The fast cation transport and superior ion selectivity of sulfonated PIM membranes are desirable for their practical application as a membrane for aqueous organic redox flow batteries. Here, we demonstrate the application of these membranes using a typical alkaline quinone flow batteries exploiting the reversible redox

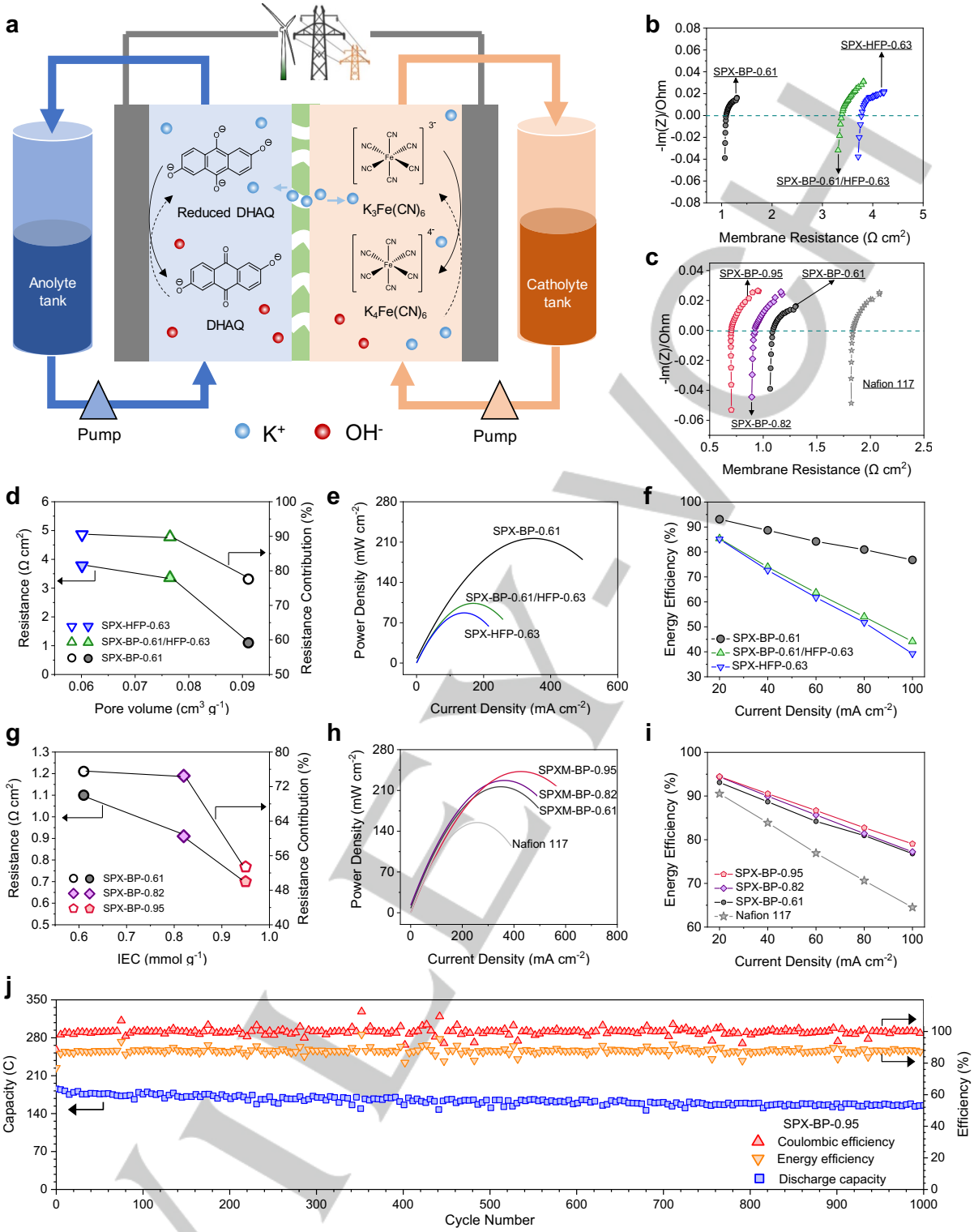

Figure 5. Performance of $K_4[Fe(CN)_6]$/DHAQ aqueous organic redox flow battery assembled with SPX-HFP, SPX-BP or Nafion 117. (a) Schematic illustration of a $K_4[Fe(CN)_6]$/DHAQ aqueous organic redox flow battery. (b) EIS spectra of membranes from SPX-HFP-0.63, SPX-BP-0.61, and their blend (50:50). (c) EIS spectra of Nafion 117 and membranes from SPX-BP with IEC value of 0.61, 0.82, or 0.95 mmol g^{-1}. The EIS spectra were collected on a Biologic-BCS 815 battery testing platform, in $K_4[Fe(CN)_6]$/DHAQ flowing cells at 50% SOC. Membrane resistance is revealed by the high-frequency area-specific resistance (AC-ASR). Membrane resistance and its contribution to the area-specific resistance of the entire cell (the ratio of AC-ASR to polarization ASR, as determined from the slope of voltage-current curves at 0 mA cm^{-2} and at 50% SOC) as functions of micropore volume of sulfonated microporous polymers (d) and IEC (g). Power density (e, h) and energy efficiency (f, i) of $K_4[Fe(CN)_6]$/DHAQ cells assembled with Nafion 117, membranes from SPX-HFP-0.63, SPX-BP-0.61, their blend, or membranes from SPX-BP with IEC value of 0.61, 0.82, or 0.95 mmol g^{-1}, as functions of current density. Power density was measured via linear sweeping voltammetry at ~100% SOC. For each current density, 10 consecutive cycles were conducted. (j) Long-term galvanostatic cycling of a $K_4[Fe(CN)_6]$/DHAQ cell assembled with SPX-BP-0.95 (to ensure clarity, full data set can be found in Figure S20) at 60 mA cm^{-2}. All experiment was carried out at ambient temperature, in an Ar-filled glovebox.

reactions of $K_4[Fe(CN)_6]$ and DHAQ molecules in aqueous electrolytes (Figure 5a).[2c] Using a laboratory scale RFB flow cell, the electrolytes were pumped on opposite sides of the ion-selective membrane, combining or releasing electrons at the carbon electrodes with K^+ ions being transferred forwards and backwards to balance the charge. The membrane resistance can be reflected by the high-frequency area-specific resistance (ASR) of a cell and, to a large extent, this value determines the RFB power capability and energy efficiency.

To demonstrate the effect of intrinsic microporosity on the areal-specific resistance of sulfonated polymer membranes, we prepared a series of membranes with varied porosity and a similar IEC value of around 0.6 mmol g^{-1}. Three typical membranes, SPX-HFP-0.63, SPX-BP-0.61/HFP-0.63 (50:50 blends), and SPX-BP-0.61 show micropore volume of 0.061 cm^3 g^{-1}, 0.076 cm^3 g^{-1}, and 0.091 cm^3 g^{-1}, as derived from CO_2 adsorption isotherms (Figures S16). The ASR of SPX-HFP-0.63, SPX-BP-0.61/HFP-0.63 (50-50) is 3.78 Ω cm^2 and 3.36 Ω cm^2, respectively and it drops dramatically to 1.10 Ω cm^2 for SPX-BP-0.61 (Figure 5b, Figure S17). Accordingly, the contribution of membrane resistance to the whole direct-current cell resistance as derived from polarization curves is significantly reduced from 90.5%, to 89.8% and to 75.5% (Figure 5d, Table S5).

To further study the effect of IEC on the membrane transport resistance, we prepared porous SPX-BP membranes with the IEC value of 0.61, 0.82, and 0.95 mmol g^{-1}. As the IEC increases from 0.61 to 0.95 mmol g^{-1}, the area-specific resistance drops from 1.10 Ω cm^2, to 0.70 Ω cm^2 (Figure 5c), contributing to 75.5%, 74.5% and 53.4% of the whole direct-current cell resistance (Figure 5g, Figure S17 and S18). In contrast, a $K_4[Fe(CN)_6]$/DHAQ cell assembled with Nafion 117 membrane gives a membrane resistance of 1.83 Ω cm^2 (Figure 5c) which contributes to 90% of the whole direct-current cell resistance (2.03 Ω cm^2 at 50% SOC, Figure S19).

Decreased membrane resistance leads directly to elevated cell power density. Peak power density of a $K_4[Fe(CN)_6]$/DHAQ cell assembled with SPX-HFP-0.63, our sulfonated polymer membrane with the lowest microporosity and the lowest IEC, is 87 mW cm^{-2}, which jumps to 243 mW cm^{-2} for the otherwise identical cell assembled with SPX-BP-0.95, our sulfonated polymer membrane with the highest microporosity and the highest IEC (Figure 5e and 5h, Figure S17-S18, Table S5). The highest peak power density obtained for SPX-BP-0.95 is ~50% greater than that of the otherwise identical Nafion 117 cell. (Figure 5h, Figure S19)

A similar trend is observed for the energy efficiency of the $K_4[Fe(CN)_6]$/DHAQ cells assembled with either our sulfonated polymer membrane or the benchmark Nafion 117. At all current densities, the cell shows higher energy efficiency when the membrane is more porous and when the IEC value is higher (Figure 5f and 5i, Figure S17-S18, Table S5). For the most porous SPX-BP-0.95 with the highest IEC, an energy efficiency of 94.5% is obtained at 20 mA cm^{-2} and it decreases to 79.0% at 100 mA cm^{-2}, which is significantly higher than that for an otherwise identical cell assembled with Nafion 117 (64.5% at 100 mA cm^{-2}, Figure 5i, Figure S19).

The high selectivity of K^+ over $[Fe(CN)_6]^{4-}$ and $DHAQ^{2-}$ (Figure 4d) and the low membrane resistance of SPX-BP-0.95 maintained a coulombic efficiency of >99% for the cell and a round-trip energy efficiency of 87.9% over 1000 consecutive charging and discharging cycles (Figure 5j, Figure S20). This value is much greater than that from the otherwise identical cell using Nafion 117 as membrane (~75%, Figure S19), that reported for a sulfonated poly (ether ether ketone) membrane (66.2%)[23]or for a Nafion 212 membrane (59.2%)[23] and even higher than that from a much thinner Nafion 211 membrane (25.4 μm thick, 84%).[2c] The SPX-BP-0.95 cell exhibited a capacity retention rate of 99.98% per cycle, or a temporal retention rate of 99.95% per hour (Figure 5j). No obvious DHAQ crossover was found after cycling as demonstrated by cyclic voltammograms (CV) measurements (Figure S21). In addition it was found that only 7.70 % of the capacity loss is due to electrolyte crossover across the SPX-BP-0.95, as determined by measuring the concentration of ferrocyanide/ferricyanide in DHAQ solution during cell cycling (Figure S22, Table S6). In contrast, electrolyte crossover contributes 8.10 % to the total capacity loss per hour for the otherwise identical cell using Nafion 117, owing to the higher electrolyte crossover rate (Figure S22, Table S6). Therefore, the small loss of capacity is mainly caused by electrolyte degradation.[2a, 24] These results demonstrate the great potential of sulfonated PIM membranes for applications in new generations of organic redox flow batteries.

Preliminary assessment of the newly-developed membranes for use in PEM fuel cells was achieved using a typical SPX-BP-0.95 membrane, in combination with Pt/C catalysts on the cathode and the anode (Figure S23a). Polarization curves of the cell at 80 °C showed that the H_2/O_2 PEMFC assembled with SPX-BP-0.95 delivered a maximum power output of 370 mW cm^{-2}, which is slightly higher than that from the same cell using a Nafion 117 membrane (348 mW cm^{-2}) (Figure S23b). The cell assembled with SPX-BP-0.95 provided stable power output over 6 hours at 80 °C, 0.5 V before the measurement was manually terminated (Figure S23c). These results show promise that the highly proton conductive sulfonated microporous membranes can also deliver high power output and stable performance in PEM fuel cells.

Conclusion

In summary, we propose a new strategy for the production of cation exchange membranes, by exploiting sulfonated polymers with rigid and contorted backbones that limit the conformation freedom and the efficient packing of polymer chains, generating confined ion channels that enable fast and selective ion transport. This is confirmed for a series of solution-processable sulfonated polyxanthene membranes that show high proton and potassium conductivity and high selectivity towards redox active anions. The facilitated ion transport significantly boosts the performance of energy conversion/storage devices, enabling the efficient and stable operation of fuel cells and redox flow batteries. This is reflected by the much lower membrane resistance and its reduced contribution to the whole system resistance, which increases energy efficiency dramatically, as demonstrated in the continued cycling of RFB flowing cells and the power density of both RFB and PEM fuel cells. The advantage of exploiting shape-persistent sulfonated PIM polymers as cation exchange membrane scaffolds includes their ease of synthesis, solution processability, ability to fine-tuned their structure, and their well-defined subnanometer channels. This is in sharp contrast to that of traditional cation exchange membranes with phase separation morphology, where the ion channels are flexible and dynamically

formed. Ion transport in our newly-developed cation exchange membranes presents both fast transport and high ionic selectivity due to the formation of smaller channels and hence greater electrostatic interaction between ions and polymer functional groups. We expect that the concept of designing cation exchange membrane and synthetic approach established in this work is general and can be applied to develop further examples of ion exchange membranes for a wide range of energy application as well as environmental processes, including but not limited to, electrodialysis, salinity gradient power generation, and ion extraction.

Acknowledgements

This work was supported by the National Natural Science Foundation of China (Nos. 21922510, 21878281, 91534203 and 21720102003), the DNL Cooperation Fund, CAS (DNL201910), the Engineering and Physical Sciences Research Council (EPSRC, UK), the Horizon 2020/FP7 Framework Program under grant agreement no. 608490, project M^4CO2., and ERC starting grant NanoMMES. The numerical calculations were performed on the supercomputing system in the Supercomputing Center at the University of Science and Technology of China. A.W. acknowledges a full PhD scholarship funded by Department of Chemical Engineering at Imperial College. R.T. acknowledges a full PhD scholarship funded by China Scholarship Council. Q.S. acknowledges the financial support by Imperial College Department of Chemical Engineering Start-up Fund, and seed-funding from EPSRC centres CAM-IES and Energy SuperStore (UK Energy Storage Research Hub).

Keywords: polymers of intrinsic microporosity • ion exchange membrane • energy conversion and storage • fuel cell • flow battery

[1] D. M. Davies, M. G. Verde, O. Mnyshenko, Y. R. Chen, R. Rajeev, Y. S. Meng, G. Elliott, *Nat. Energy* **2019**, *4*, 42-50.

[2] a) A. Hollas, X. Wei, V. Murugesan, Z. Nie, B. Li, D. Reed, J. Liu, V. Sprenkle, W. Wang, *Nat. Energy* **2018**, *3*, 508-514; b) K. Lin, R. Gómez-Bombarelli, E. S. Beh, L. Tong, Q. Chen, A. Valle, A. Aspuru-Guzik, M. J. Aziz, R. G. Gordon, *Nat. Energy* **2016**, *1*, 16102; c) K. Lin, Q. Chen, M. R. Gerhardt, L. Tong, S. B. Kim, L. Eisenach, A. W. Valle, D. Hardee, R. G. Gordon, M. J. Aziz, M. P. Marshak, *Science* **2015**, *349*, 1529; d) M. Park, J. Ryu, W. Wang, J. Cho, *Nat. Rev. Mater.***2016**, *2*, 16080.

[3] J. A. Turner, *Science* **2004**, *305*, 972-974.

[4] Z. P. Cano, D. Banham, S. Ye, A. Hintennach, J. Lu, M. Fowler, Z. Chen, *Nat. Energy* **2018**, *3*, 279-289.

[5] R. M. Darling, K. G. Gallagher, J. A. Kowalski, S. Ha, F. R. Brushett, *Energy Environ. Sci.* **2014**, *7*, 3459-3477.

[6] K. Schmidt-Rohr, Q. Chen, *Nat. Mater.* **2007**, *7*, 75.

[7] D. W. Shin, M. D. Guiver, Y. M. Lee, *Chem. Rev.* **2017**, *117*, 4759-4805.

[8] a) N. B. McKeown, P. M. Budd, *Chem. Soc. Rev.* **2006**, *35*, 675-683; b) Z.-X. Low, P. M. Budd, N. B. McKeown, D. A. Patterson, *Chem. Rev.* **2018**, *118*, 5871-5911; c) R. Tan, A. Wang, R. Malpass-Evans, R. Williams, E. W. Zhao, T. Liu, C. Ye, X. Zhou, B. P. Darwich, Z. Fan, L. Turcani, E. Jackson, L. Chen, S. Y. Chong, T. Li, K. E. Jelfs, A. I. Cooper, N. P. Brandon, C. P. Grey, N. B. McKeown, Q. Song, *Nat. Mater.* **2019**, *19*, 195-202; d) M. J. Baran, M. N. Braten, S. Sahu, A. Baskin, S. M. Meckler, L. Li, L. Maserati, M. E. Carrington, Y.-M. Chiang, D. Prendergast, B. A. Helms, *Joule* **2019**, *3*, 2968-2985.

[9] a) I. S. Chae, T. Luo, G. H. Moon, W. Ogieglo, Y. S. Kang, M. Wessling, *Adv. Energy Mater.* **2016**, *6*, 1600517; b) L. Qi, L. Shang, K. Wu, L. Qu, H. Pei, W. Li, L. Zhang, Z. Wu, H. Zhou, N. B. McKeown, W. Zhang, Z. Yang, *Chem. Eur. J.* **2019**, *25*, 12052-12057; c) C. Li, A. L. Ward, S. E. Doris, T. A. Pascal, D. Prendergast, B. A. Helms, *Nano Lett.* **2015**, *15*, 5724-5729; d) S. E. Doris, A. L. Ward, P. D. Frischmann, L. Li, B. A. Helms, *J. Mater. Chem. A* **2016**, *4*, 16946-16952; e) G. H. Moon, H. J. Kim, I. S. Chae, S. C. Park, B. S. Kim, J. Jang, H. Kim, Y. S. Kang, *Chem. Commun.* **2019**, *55*, 6313-6316.

[10] Z. Yang, R. Guo, R. Malpass-Evans, M. Carta, N. B. McKeown, M. D. Guiver, L. Wu, T. Xu, *Angew. Chem. Int. Ed.* **2016**, *55*, 11499-11502.

[11] J. Wang, Y. Zhao, B. P. Setzler, S. Rojas-Carbonell, C. Ben Yehuda, A. Amel, M. Page, L. Wang, K. Hu, L. Shi, S. Gottesfeld, B. Xu, Y. Yan, *Nat. Energy* **2019**, *4*, 392-398.

[12] B. G. Kim, D. Henkensmeier, H.-J. Kim, J. H. Jang, S. W. Nam, T.-H. Lim, *Macromol. Res.* **2013**, *22*, 92-98.

[13] a) L. I. Olvera, M. G. Zolotukhin, O. Hernandez-Cruz, S. Fomine, J. Cardenas, R. L. Gavino-Ramirez, F. A. Ruiz-Trevino, *ACS Macro Lett.* **2015**, *4*, 492-494; b) L. I. Olvera, M. Rodriguez-Molina, F. A. Ruiz-Trevino, M. G. Zolotukhin, S. Fomine, J. Cardenas, R. Gavino, L. Alexandrova, R. A. Toscana, E. Martinez-Mercado, *Macromolecules* **2017**, *50*, 8480-8486.

[14] N. Du, H. B. Park, G. P. Robertson, M. M. Dal-Cin, T. Visser, L. Scoles, M. D. Guiver, *Nat. Mater.* **2011**, *10*, 372.

[15] R. Borup, J. Meyers, B. Pivovar, Y. S. Kim, R. Mukundan, N. Garland, D. Myers, M. Wilson, F. Garzon, D. Wood, P. Zelenay, K. More, K. Stroh, T. Zawodzinski, J. Boncella, J. E. McGrath, M. Inaba, K. Miyatake, M. Hori, K. Ota, Z. Ogumi, S. Miyata, A. Nishikata, Z. Siroma, Y. Uchimoto, K. Yasuda, K.-i. Kimijima, N. Iwashita, *Chem. Rev.* **2007**, *107*, 3904-3951.

[16] M.-H. Kim, J. D. Londono, A. Habenschuss, *J. Polym. Sci., Part B: Polym. Phys.* **2000**, *38*, 2480-2485.

[17] G. M. Geise, D. R. Paul, B. D. Freeman, *Prog. Polym. Sci.* **2014**, *39*, 1-42.

[18] a) T. J. Peckham, S. Holdcroft, *Adv. Mater.* **2010**, *22*, 4667-4690; b) L. C. H. Moh, J. B. Goods, Y. Kim, T. M. Swager, *J. Membr. Sci.* **2018**, *549*, 236-243.

[19] a) K. D. Kreuer, A. Rabenau, W. Weppner, *Angew. Chem. Int. Ed.* **1982**, *21*, 208-209; b) D. Dong, W. Zhang, A. C. T. van Duin, D. Bedrov, *J. Phys. Chem. Lett.* **2018**, *9*, 825-829.

[20] E. R. Nightingale, *J. Phys. Chem.* **1959**, *63*, 1381-1387.

[21] T. Luo, S. Abdu, M. Wessling, *J. Membr. Sci.* **2018**, *555*, 429-454.

[22] Z. Siwy, I. D. Kosinska, A. Fulinski, C. R. Martin, *Phys. Rev. Lett.* **2005**, *94*, 048102.

[23] D. De Porcellinis, B. Mecheri, A. D'Epifanio, S. Licoccia, S. Granados-Focil, M. J. Aziz, *J. Electrochem. Soc.* **2018**, *165*, A1137-A1139.

[24] a) A. E. Wendlandt, S. S. Stahl, in *Liquid Phase Aerobic Oxidation Catalysis: Industrial Applications and Academic Perspectives*, **2016**, pp. 219-237; b) D. G. Kwabi, K. Lin, Y. Ji, E. F. Kerr, M.-A. Goulet, D. DePorcellinis, D. P. Tabor, D. A. Pollack, A. Aspuru-Guzik, R. G. Gordon, M. J. Aziz, *Joule* **2018**, *2*, 1894-1906; c) J. Luo, A. Sam, B. Hu, C. DeBruler, X. L. Wei, W. Wang, T. L. Liu, *Nano Energy* **2017**, *42*, 215-221.

Entry for the Table of Contents

Sulfonated microporous polymer membranes with fast and selective ion transport for electrochemical energy con-version and storage

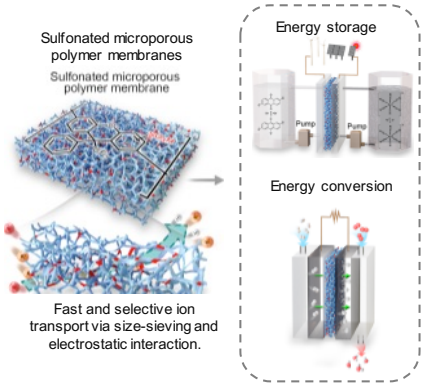

Sulfonated polyxanthene membranes with both intrinsic microporosity and conductive functionality were synthesized, exhibiting remarkable ion conductivity and high selectivity towards redox-active anions. They significantly enhance the performance of redox flow battery and hydrogen fuel cell, demonstrating the design concept established here is broadly applicable.